J Electroceram (2009) 23:564–571
DOI 10.1007/s10832-008-9548-5

Effects of co-doped CaO/MnO on the piezoelectric/dielectric properties and phase transition of lead-Free $(Bi_{0.5}Na_{0.5})_{0.94}Ba_{0.06}TiO_3$ piezoelectric ceramics

Man-Soon Yoon · Young-Geun Lee · Soon-Chul Ur

Received: 30 May 2007 / Accepted: 27 August 2008 / Published online: 10 September 2008

Abstract The piezoelectric properties of $(1-x)(Bi_{0.5}Na_{0.5})TiO_3$-$xBaTiO_3$ ceramics were reported and their piezoelectric properties reach extreme values near the MPB (about x= 0.06). The X-ray analysis of $(Bi_{0.5}Na_{0.5})_{0.94}Ba_{0.06}TiO_3$ ceramics for all compositions exhibited a pure perovskite structure without any secondary phase. Within a certain ratio of contents, the co-doped ceramics enhanced piezoelectric coefficient (d_{33}), lowered the dielectric loss, and increased the sintered density. The temperature dependence of relative dielectric permittivity (K_{33}^T) reveals that the solid solutions experience two phase transitions, ferroelectric to anti-ferroelectric and anti-ferroelectric to relaxor ferroelectric, which can be proven by P-E hysteresis loops at different temperatures. In addition, the specimen containing 0.04/0.01 wt.% CaO/MnO showed that the coercive field E_c was a minimum value of 26.7 kV/cm, while the remnant polarization P_r was a maximum value of 38.7 μC/cm^2, corresponding to the enhancement of piezoelectric constant d_{33} of 179 pC/N, electromechanical coupling factor k_p of 37.3%, and relative dielectric permittivity K_{33}^T of 1137. $(Bi_{0.5}Na_{0.5})_{0.94}Ba_{0.06}TiO_3$ ceramics co-doped with CaO/MnO were considered to be a new and promising candidate for lead-free piezoelectric ceramics owing to their excellent piezoelectric/dielectric properties, which are superior to an un-doped BNBT system.

Keywords BNBT · Co-doping · CaO/MnO · Piezoelectric · Dielectric · Phase transition

M.-S. Yoon (✉) · Y.-G. Lee · S.-C. Ur
Department of Materials Science and Engineering/Research Center for Sustainable Eco-Devices and Materials (ReSEM), Chungju National University,
Chungbuk 380-702, Korea
e-mail: msyoon@cjnu.ac.kr

1 Introduction

Perovskite piezoelectric ceramics containing lead oxide such as Pb(Ti, Zr)O_3 (PZT) are now widely used in piezoelectric devices because of their excellent piezoelectric properties [1]. However, recently emerged environmental issues such as the restriction of WEEE (Waste Electrical and Electronic Equipment) and RoHS (Restriction of Hazardous Substances) will prohibit us from using lead oxide in the near future due to their toxicity. In an approach to acclimate ourselves to the recent ecological consciousness trends [2, 3], a lead-free piezoelectric material, bismuth sodium barium titanate, was considered as an environment-friendly alternative for a PZT system.

Since Bismuth sodium titanate, $Bi_{0.5}Na_{0.5}TiO_3$ (abbreviated as BNT), was discovered by Smolenskii et al. in 1960 [4], BNT is considered to be an excellent candidate as a key material of lead-free piezoelectric ceramics because BNT is strongly ferroelectric. Besides, pure BNT shows the characteristics of diffuse phase transition (DPT). The BNT ceramic exhibits a large remnant polarization, P_r=38 μC/cm^2, a high Curie temperature (T_c=320 °C). Also, the dielectric properties display a very interesting anomaly wherein the low temperature phase transition at 200 °C marks the transition from ferroelectric to antiferroelectric [5]. However, because of its high coercive field, E_c=73 kV/cm, and relatively large conductivity, the pure BNT is difficult to be poled and cannot be a good piezoelectric material. These problems were then improved by forming solid solutions with $BaTiO_3$(BT), $Bi_{0.5}K_{0.5}TiO_3$, $KNbO_3$, $NaNbO_3$, $(Sr_aPb_bCa_c)TiO_3$, $BiFeO_3$, $BiScO_3$, etc [6–13]. Among these systems, bismuth sodium barium titanate $(Bi_{0.5}Na_{0.5})_{1-x}Ba_xTiO_3$ (BNBT) has been widely investigated by many researchers [7, 14–15]. The morphotropic phase boundary (MPB) of this solid solution system is near

x=0.06, where the materials show enhanced piezoelectric, dielectric performances. Takenaka et al. [7] have reported that the composition of $(Bi_{0.5}Na_{0.5})_{0.94}Ba_{0.06}TiO_3$, which is near the MPB, has relatively good piezoelectric properties of k_{33}=0.55, k_{31}=0.19, d_{33}=125pC/N. However, this composition has a higher coercive electric field and medium piezoelectiric constant. These properties were afterward promoted by a few research group [16–18]. It was believed that substitution at A-site or B site may induce soft or hard properties in a piezoelectric material by forming cations or oxygen vacancies, respectively. Several kinds of cations like La^{+3}, Nb^{+5}, Co^{+3}, Mn^{+2}, etc. were tested to further modify BNT-based piezoelectric ceramics [19–22]. More interestingly, Takenaka et al. [7] demonstrated that BNBT6 underwent phase transition from ferroelectric to antiferroelectric state at ~120 °*C* and subsequent transition to paraelectric state at ~270 °*C*.

The main purpose of this study is to synthesize a $(Bi_{0.5}Na_{0.5})_{0.94}Ba_{0.06}TiO_3$ composition and to rationalize the effect of co-doping with CaO/MnO on the piezoelectric/dielectric properties and phase transition behavior in the BNBT system.

To achieve the main purpose of our study, we (1) investigate the piezoelectric/dielectric properties and microstructure morphology in a CaO/MnO co-doped BNBT system, (2) analyze the effect of CaO/MnO additives on phase transition and (3) correlate these phase transition with *P-E* hysteresis loop.

2 Experimental procedure

Perovskite $(Bi_{0.5}Na_{0.5})_{0.94}Ba_{0.06}TiO_3$ (abbreviated as BNBT6) (0.05−x) wt.% CaO−x wt.% MnO $(0.01 \leq x \leq 0.04)$ [sometimes abbreviated as BNBT6(x)] ceramics were fabricated using a conventional ceramic processing technique. Raw materials of analytical-reagent (AR) grade Bi_2O_3, Na_2CO_3, $BaCO_3$, TiO_2, $CaCO_3$, and $MnCO_3$ were weighed and ball milled with ZrO_2 media in distilled water for 24 h. The dried powder mixtures were sieved under 100 mesh and then calcined at 850 °*C* for 2 h. An additional ball-milling step was added to ensure a fine particle size before sintering. The dried powders were first pressed as disks (φ 15 mm) and then cold-isostatically pressed under 190 MPa pressure The pressed pellets were sintered at 1170 °*C* for 2 h with a heating rate of 3 °*C* /min. The sintered specimens were then polished to obtain parallel surfaces. Phase analyses for the sintered bodies were carried out using an X-ray diffractometer (XRD; Rigaku D/MAX-2500H), and microstructures were investigated using a scanning electron microscope (SEM; Hitachi S-2400). In order to measure the electrical properties, silver paste was coated to form electrodes on both sides of the sample, and then subsequently fired at 650 °*C* for 20 min. The dielectric and piezoelectric properties were measured using an impedance/gain phase analyzer (HP-4194A) after poling under 7.5 kV/mm at 90 °*C* in a silicone oil bath for 40 min. Piezoelectric properties were calculated using a resonance/anti-resonance measurement method [23]. Temperature dependence of the dielectric constant and dissipation factor over a range from room temperature to 350 °*C* was measured using an automated system at various frequencies between 1 kHz and 100 kHz, whereby HP-4194A and a temperature-control box (Lindberg tube furnace) were controlled by a desk-top computer system. The temperature was measured using a Keithley 740 thermometer via a K-type thermocouple mounted near the sample. The electromechanical coupling factor (K_p) at various temperature (30~200 °*C*) was measured by recording the resonance and anti resonance frequencies of sample with HP-4194A. To obtain the information on the temperature-dependent phase transition, the induced electric polarization at various temperatures was measured using a Precision LC system (Radiant Technology Model: 610E).

3 Results and discussion

3.1 Effects of CaO/MnO co-doping on crystal structure and microstructure

Figure 1 shows the X-ray diffraction patterns for pure BNBT6 and doped BNBT6 in the 2Θ range of 20° to 80°. A full stabilization of perovskite phase was achieved for the whole range of the composition studied. Without CaO/MnO co-doping, the pure BNBT6, labeled (a) in this case, shows the coexistence of tetragonal and rhombohedral symmetry. A comparison of the result of Fig. 1(a) with that of Fig. 1(b) indicate that the (002) peak is suppressed and the rhombohedral phase increases as increasing the amount of Ca ion doping more than that of Mn ion doping. It can be explained by the fact that the lattice aniosotropy, as Ca^{+2} with an ionic radius of 1.00 Å substituted into Bi^{+3} or Na^{+1} with an ionic radius of 1.03 Å, 1.02 Å, respectively, is reduced [24]. On the contrary, note that a splitting of (200) and (002) increases more with an increase in the amount of added Mn ion as shown in Fig. 1(b)~ (d).

The mechanism for the effect of MnO is very complicate. Mn ion possibly exists in the BNBT with multi-valence states: Mn^{+2} in radius of 0.67 Å, Mn^{+3} in radius of 0.58 Å and Mn^{+4} in radius of 0.53 Å [24]. It can be noted that the peak splitting appeared at (002) and (200) plane positions as increasing the amount of Mn ion doping. It is also shown that tetragonality (degree of tetragonal peak separation) increases with increasing MnO content. It can be explained by the fact that Mn^{+2} with an ionic radius of 0.67 Å are substituted into the Ti^{+4} with an ionic radius of 0.61 Å [24]. Since Mn is divalent whereas

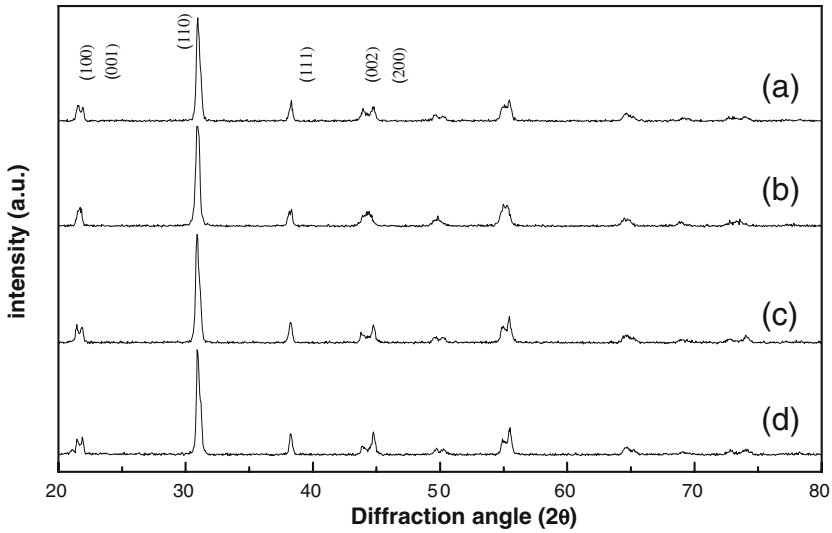

Fig. 1 XRD patterns as a function of CaO/ MnO contents in BNBT6: (*a*) 0, (*b*) 0.04/0.01, (*c*) 0.02/0.03, (*d*) 0.01/0.04 wt.%

Ti is tetravalent, the Mn behaves as an acceptor dopant. Therefore, the acceptor doping with Mn ions would be expected to compensate the charge imbalance resulting from the formation of oxygen vacancies. It has been known that oxygen vacancies are the main cause of domain wall clamping [25]. The substitution of relatively large-sized Mn^{+2} ion with the relatively small-sized Ti^{+4} ion leads to increase the tetragonality and this in turn accompanies (002) and (200) peak separation the more widely, suggesting an increased relative stability of the tetragonal phase.

The microstructures of the sintered pure BNBT6 and CaO/MnO modified samples were observed by SEM, and the micrographs of the samples containing various amount of CaO/MnO (0, 0.04/0.01, 0.02/0.03, 0.01/0.04 wt.%) are shown in Fig. 2. It is evident that the addition of CaO/MnO causes a significant change in the grain size and morphology, increasing the sintering density to 5.86 g/cm^3, compared with a density of 5.67 g/cm^3 in a pure BNBT6 system. It seems that the CaO/MnO addition prohibits grain growth. The grain size decreases with increasing the MnO content; in particular, morphologies of BNBT6 containing CaO/MnO change from a square pillar shape to a polyhedral shape. Therefore, the observed equilibrium shape change seems to be closely related with the increase of the sintering density.

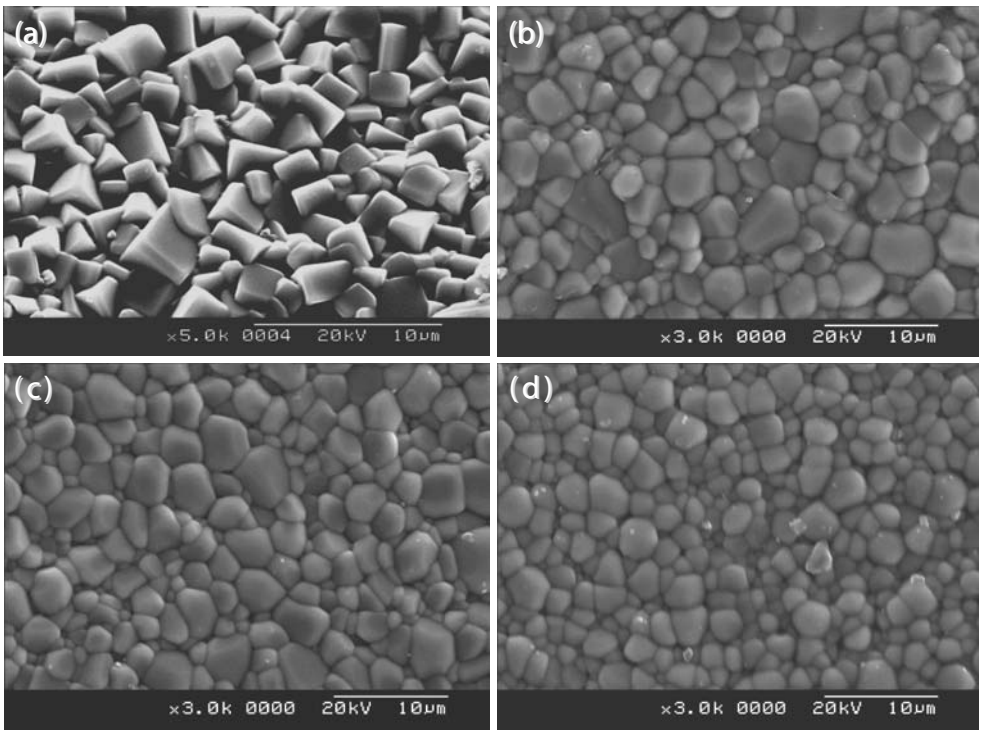

Fig. 2 SEM micrograph as a function of CaO/MnO content in BNBT6 sintered at 1170 °*C* for 2 h: (**a**) 0, (**b**) 0.04/0.01, (**c**) 0.02/0.03, (**d**) 0.01/0.04 wt.%

3.2 Effects of CaO/MnO co-doping on dielectric and piezoelectric properties

The piezoelectric and dielectric properties of $(Bi_{0.5}Na_{0.5})_{0.94}$-$Ba_{0.06}TiO_3$ specimens containing various amount of CaO/MnO (0, 0.04/0.01, 0.02/0.03, 0.01/0.04 wt.%) are shown in Fig. 3(a) and (b). As shown in Fig. 3, the composition containing 0.04/0.01 wt.% CaO/MnO [BNBT6(0.01)] shows maximum values of piezoelectric constant d_{33} of 179 pC/N, electromechanical coupling factor K_p of 37.3% and relative dielectric permittivity (K_{33}^T) of 1137 compared with pure BNBT6 ceramics and which then decrease with increasing MnO content. However, the mechanical quality factor Q_m steadily increased to 180. In case of BNBT6(0.01), the effect of CaO doping becomes dominant compared with that of MnO doping. Therefore, the increase of piezoelectric and dielectric properties can be interpreted as the effect of CaO doping. It is well known that CaO is a commonly used additive for PZT ceramics for improving the piezoelectric/dielectric properties [26]. Ca ion exists in the BNBT6 structure in Ca^{+2} with a radius of 1.00 Å. In view of the radius, it is obvious that Ca^{+2} cannot enter into the B-site of BNBT6 perovskite because the radius of Ti^{+4} is 0.61 Å, but it can occupy A-site. In addition, compared to Ba^{+2} with a radius of 1.35 Å, Bi^{+3} in radius of 1.03 Å and Na^{+1} in radius of 1.02 Å are very close to that of Ca^{+2} (1.00 Å), therefore, Ca^{+2} can occupy the Bi^{+3}, Na^{+1} site easier than the Ba^{+2} site without large lattice distortion. But, when Ca^{+2} enter into the Bi-site of BNBT6 ceramics, it can make c/a reduce, and the rhombohedral phase then increases when increasing the amount of Ca^{+2} doping. On the other hands, as Ca^{+2} enter Bi^{+3} site, the charge compensation will occur by creation of oxygen vacancy. As increasing oxygen vacancy, the movement of the domain wall is restricted, resulting in a decrease of the piezoelectric and dielectric properties [26]. As mentioned above, the substitution of Bi^{+3} by Ca^{+2} cannot explain the increase of the piezoelectric and dielectric properties at 0.04/0.01 wt.% CaO/MnO. Another case is that Ca^{+2} occupy the Na^{+1} site of a BNBT6 composition. In this case, Ca^{+2} functions as a donor leading to some vacancies of the A-site in the lattice, which facilitates the movement of domain wall so as to improve the piezoelectric and dielectric properties [26]. From the above analysis, it can be concluded that in the composition where the effect of adding CaO is dominant, the piezoelectric and dielectric properties are increased as Ca^{+2} replaces Na^{+1}.

When increasing MnO content more than CaO, the dielectric properties decreased continuously as shown in Fig. 3(a). As shown in Fig. 3(b), mechanical quality factor Q_m increased steadily with increasing MnO content. Mn ions possibly exist in the BNBT6 structure in various valance states: Mn^{+2} with a radius of 0.67 Å, which is close to that of Ti^{+4}(0.61 Å). According to the principle of crystal chemistry, Mn ions are most likely to go into the B-site in a perovskite system, substituting Ti^{+4}. As discussed in the previous subsection 3.1, the increase of MnO content accompanies a significant increase of tetragonal phase. From considerations of ionic radii, it is highly probable that Mn ion occupy B-site of perovskite. As Mn^{+2} enter into the B-site, the charge compensation will occur by a creation of oxygen vacancies. It is known that oxygen vacancies are the main cause of domain clamping [25]. This clamping will restrain the movement of the domain wall and accompany a significant decrease of the piezoelectric and dielectric properties, while the mechanical quality factor steadily increases with increasing MnO content. It also matches with the hardener effect of MnO content on a traditional PZT composition [25, 26].

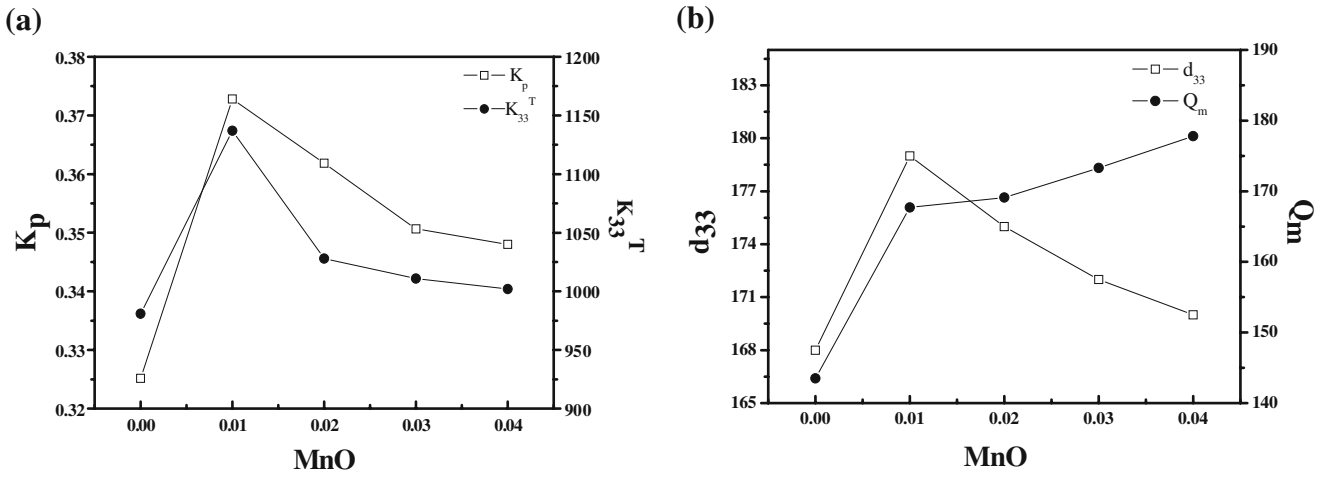

Fig. 3 Variation of piezoelectric and dielectric properties as a function of MnO content in CaO/MnO co-doped BNBT6 composition sintered at 1443 K for 2 h: (**a**) Relative dielectric permittivity (K_{33}^T) and electromechanical coupling factor (K_p) (**b**) Piezoelectric constant (d_{33}) and mechanical quality factor (Q_m)

3.3 Effects of CaO/MnO co-doping on ferroelectric to antiferroelectric phase transition

Figure 4(a)~(c) show the temperature dependence of relative dielectric permittivity (K_{33}^T), dielectric loss ($tan\delta$) of the prepoled BNBT6 and CaO/MnO doped BNBT6 ceramics at 1 kHz. It can be seen that the three phases of ferroelectric, anti-ferroelectric and relaxor ferroelectric are divided by two special temperatures.

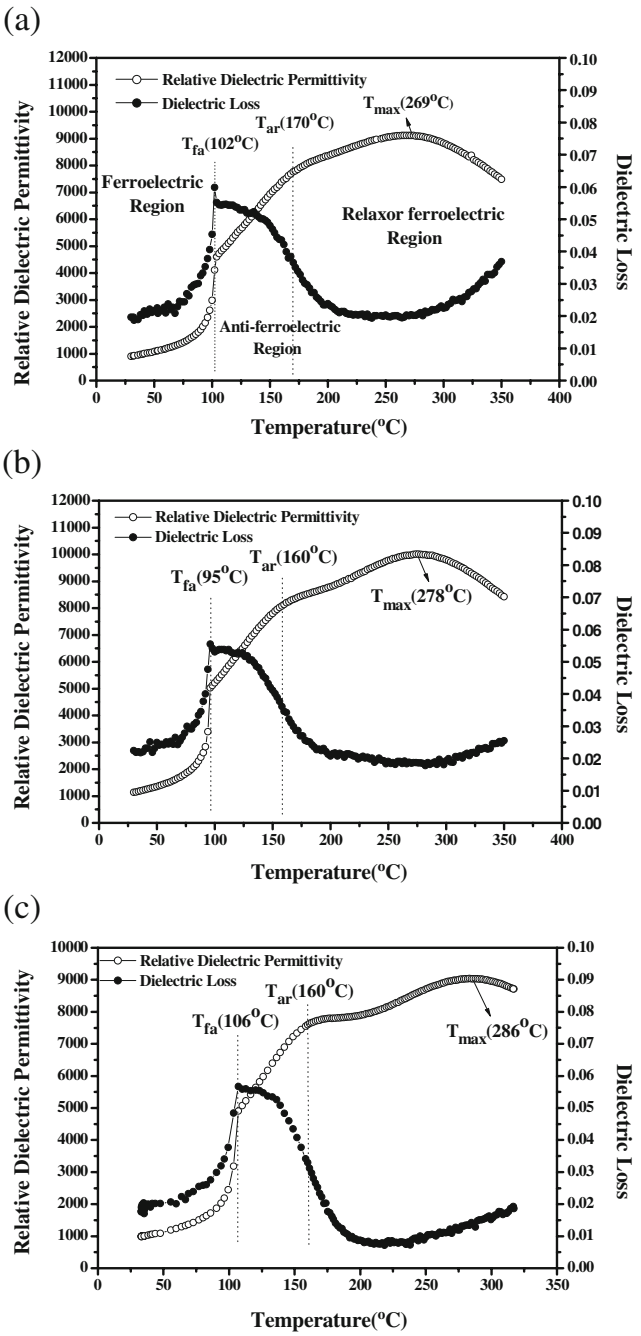

Fig. 4 Relative dielectric permittivity (K_{33}^T). And tanδ as a function of temperature for the pre-poled pure and CaO/MnO doped BNBT6 ceramics at 1 kHz: (**a**) 0, (**b**) 0.04/0.01, (**c**) 0.01 /0.04 wt. %

On heating, the specimens exhibit peak broadness near T_{max} where T_{max} is the temperature of the peak dielectric permittivity. In this work, the coexistence of Bi^{+3}, Na^{+1}, Ba^{+2} at A-site could introduce a relaxor ferroelectric behavior, which was also proved by Säid and co-workers [27, 28]. On further heating, the permittivity and tanδ sharply increases at a critical temperature, indicated as T_{fa} in Fig. 4. The subscript *fa* designates the spontaneous switching from ferro-electric to anti-ferroelectric state. As shown in Fig. 4(a), (b), (c), it was noted that with increasing the content of CaO to 0.04 wt.%, the temperatures T_{fa} decreased to 95 °*C* (T_{fa}=102 °*C* for pure BNBT6 and 106 °*C* for 0.04 wt.% MnO doped BNBT6). As discussed in the previous sections, increasing the content of CaO in the BNBT6 system enhances rhombohedral phase and domain mobility but decreases the internal stress. Therefore, the stability of ferroelectric domain can be reduced by CaO doping. This explains the observed decrease of T_{fa}. An examination of the dielectric loss indicates that there exist inflection point in tanδ vs temperature curves at $T=T_{fa}$. The temperature for the inflection in tanδ essentially coincides with T_{fa}. In addition to this, as increasing the content of MnO to 0.04 wt.%, the temperatures T_{fa} increased to 106 °*C*, the observed increase of the T_{fa} can be explained in terms of the domain wall clamping, which restrained the ferroelectric and anti-ferroelectric transition, caused by oxygen vacancies [21, 25]. In addition to this, as mentioned above, a possible substitution of Mn ion with Ti ion would lead to increase the stability of tetragonal phase, and thus, increase the internal stress. The increase in the internal stress can be effectively reduced by the formation of twin-like 90° domains having tetragonal symmetry, which increase the stability of ferroelectric state [29]. Therefore, the ferroelectric and anti-ferroelectric transition can be suppressed by MnO doping. The dielectric permittivity characteristics of pure BNBT6 and doped BNBT6 above T_{fa} suggest that there exists a transition zone between the antiferroelectric and relaxor ferroelectric state. As shown in Fig. 4(a)~(c), the dielectric permittivity responses for all specimens increase until temperature reaches at T_{ar}. After that, the tendency of the increase becomes slow and the curve begins to broaden. The subscript *ar* designates the spontaneous switching from anti-ferroelectric to relaxor ferroelectric state. To investigate the dielectric dispersion at T_{fa}, T_{ra} and T_{max}, the dielectric responses for the prepoled 0.04./0.01 wt.% CaO/MnO doped BNBT6 [i.e. BNBT6(0.01)] at various ac frequencies are presented in Fig. 5. On heating, the specimen exhibits dielectric dispersion above T_{fa}, the dielectric permittivity sharply increases at critical temperature, indicated as T_{fa}. The rapid increase in dielectric permittivity at T_{fa} is similar to that observed in normal ferroelectrics just below the Curie

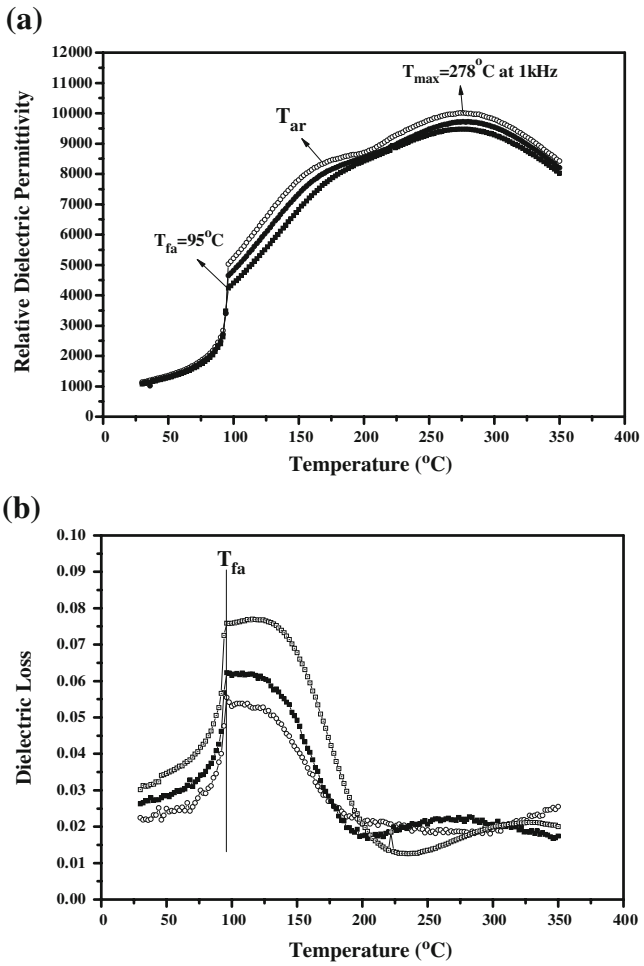

Fig. 5 Temperature dependence of relative dielectric permittivity and dielectric loss of the prepoled 0.04./0.01 wt.% CaO/MnO doped BNBT6 [i.e. BNBT6(0.01)] at various ac frequencies. The measurement frequencies from top to the bottom curve are 1 kHz, 10 kHz, 100 kHz

temperature. Therefore, it appears that, on heating, a spontaneous transformation occurs from ferroelectric to anti-ferroelectric state, i.e. ferroelectric-antiferroelectric domain switching. Moreover, a large extent of dielectric dispersion was observed in the temperature region between T_{fa} and T_{ar} (i.e. anti-ferroelectric region). As increases the frequency, the dielectric permittivity lowers and the transition temperature T_{ar} increases. From the results, the observed dielectric dispersion in anti-ferroelectric region suggests the existence of remnant polar microregions in a long-range anti-ferroelectric domain. In addition to this, an inflection points were observed near a critical temperature, marked as T_{ar} in Figs. 4 and 5 and then weakens the characteristics of dielectric dispersion over a narrow temperature range above T_{ar}. As shown in Fig. 5, increasing the temperature near T_{max}, relaxor behavior was again appeared. Therefore, this result supports that T_{ar} is related with antiferroelectric-relaxor transition. Further evidence for phase transition (ferroelectric-antiferroelectric) was obtained by examining temperature dependent planar electro-mechanical coupling coefficient (K_p). As shown Fig. 6, the temperatures of a rapid drop in K_p are exactly consistent with T_{fa}. Therefore, these results show the occurrence of ferroelectric–antiferroelectric phase transition, which corresponds with depolarization temperature.

A slow, gradual decrease in K_p above T_{fa}, together with a substantial value of K_p above T_{fa}, indicates the existence of ferroelectric domain which are remained in a anti-ferroelectric phase. The K_p diminished as the temperature increases to T_{ar}. According to the results of the Figs. 4 and 6, T_{fa} and T_{ar} seem to be closely related with ferroelectric–antiferroelectric phase transition and antiferroelectric-relaxorphase transition, respectively.

Furthermore, the phase transition is directly associated with the variation of polarization-electric field (*P-E*) hysteresis loop. The *P-E* curves for pure BNBT6 and CaO/MnO co-doped BNBT6 (freshly prepared) are presented in Fig. 7. The data were taken when the samples were heated from a room temperature and reached a desired temperature. The values of remnant polarization (P_r) and coercive field (E_c) were determined from the measured loop. From the data of hysteresis loops measured at 30 °*C*, the remnant polarization P_r for BNBT6(0.01) specimen has a maximum value of 38.7 μC/cm^2, resulting in higher value compared with the P_r of pure BNBT6 and BNBT6(0.04) [P_r=24.6 μC/cm^2 for pure BNBT6 and 36.8 μC/cm^2 for BNBT6(0.04)] and the shape of loop corresponds to a typical polarization curve for a normal ferroelectric below the Curie temperature. In addition to this, when the amount of CaO contents increases at 0.04 wt.% [BNBT6(0.01)], the

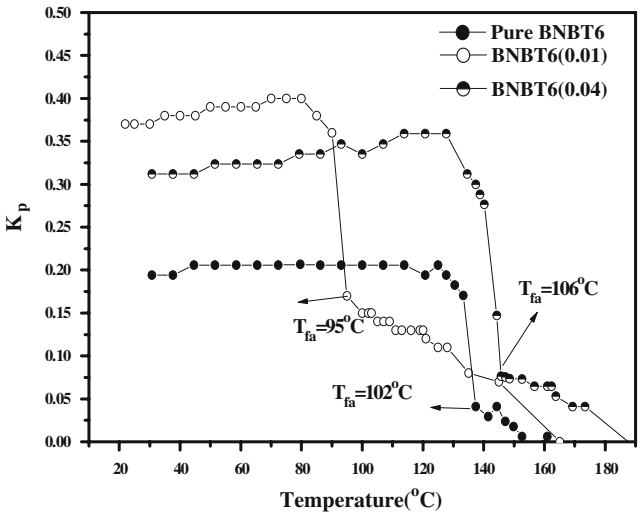

Fig. 6 Temperature dependence of planar electro-mechanical coupling coefficient (K_p)

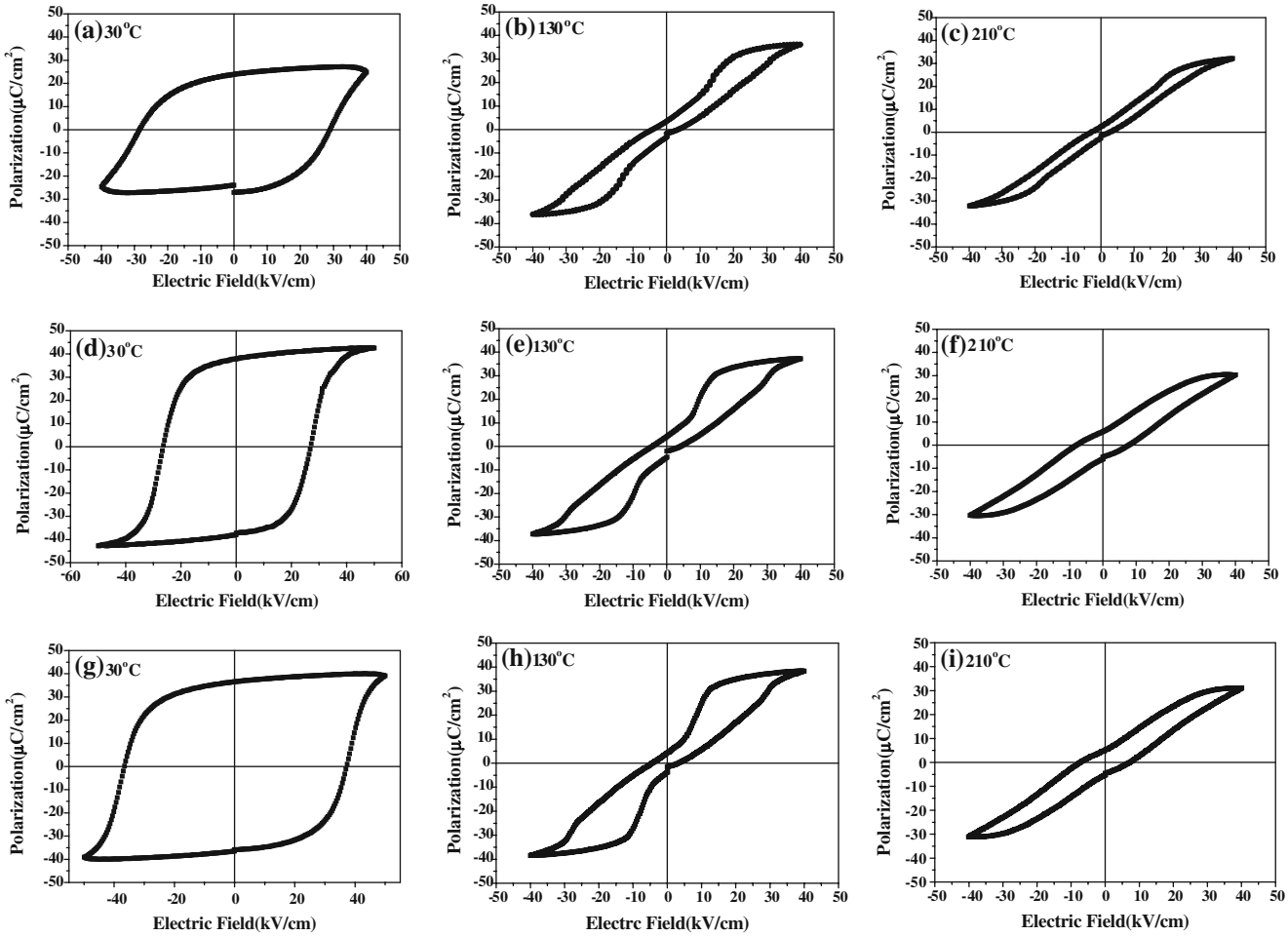

Fig. 7 Electric field-induced polarization(P_r) of freshly prepared pure and CaO/MnO doped BNBT6 ceramics at various temperature: (**a**)–(**c**) pure BNBT(6), (**d**)–(**f**) co-doped BNBT6(0.01), (**g**)–(**i**) co-doped BNBT6(0.04)

coercive field *E*c has a minimum value of 26.7 kV/cm. As mentioned previously, it can be expected that CaO dopant behaviors as a donor in BNBT6 matrix, probably generating vacancies of A-site cations. The soft properties are thus induced, concerning a reduced E_c and improved d_{33}. However, in the case of increasing MnO content to 0.04 wt.% [BNBT6(0.04)], the coercive field E_c has a maximum value of 37.5 kV/cm [E_c=28.5 μC/cm^2 for pure BNBT6 and 26.7 μC/cm^2 for BNBT6(0.04)]. These results were in accord with a previous analysis of the piezoelectric/dielectric properties as a clamping effect of oxygen vacancy. When the temperature increases to 130 °*C*, which temperature lies in anti-ferroelectric region, the all specimens show a double hysteresis loop, reflecting the appearance of an antiferroelectric state. At a further elevated temperature of 210 °*C* (for T_{armax}), *P-E* curves of all specimens show a relaxor behavior. Therefore, these P-E observations at various temperature demonstrate that T_{fa} and T_{ar} is directly associated with the above mentioned phase transition phenomena.

4 Conclusions

The effect of co-doping with CaO/MnO on the piezoelectric properties, microstructure and phase transition in the BNBT 6 system was systematically investigated. The X-ray analysis of $(Bi_{0.5}Na_{0.5})_{0.94}Ba_{0.06}TiO_3$ ceramics for a various amount of dopants exhibited a pure perovskite structure without any secondary phase. The rhombohedral phase increased as increasing the amount of Ca^{+2} doping more than that of Mn^{+2} doping. On the contrary, addition of Mn^{+2} led to the (200) and (002) peak separating more widely, suggesting an increased relative stability of the tetragonal phase. The microstructures of the sintered pure BNBT6 and CaO/MnO modified samples were also observed by SEM. It was evident that the addition of CaO/MnO caused a significant change in the grain size and morphology, increasing the sintering density. The composition containing 0.04/0.01 wt.% CaO/MnO [BNBT6 (0.01)] showed maximum values of piezoelectric constant, electromechanical coupling factor and relative dielectric

permittivity and which then decrease with increasing MnO content. Furthermore, The $K_{33}{}^{T}$-temperature curves of the compositions used in this study exhibited the unique phase transitions. On heating, a spontaneous transformation occurred from ferroelectric to antiferroelectric state. In addition to this, the spontaneous switching from antiferroelectric to relaxor ferroelectric state was also observed. Further evidence for phase transition was obtained by examining temperature dependent planar electro-mechanical coupling coefficient and polarization-electric field (*P-E*) hysteresis loop. From the results, T_{fa} and T_{ar} were closely related with ferroelectric-antiferroelectric and antiferroelectric-relaxor phase transition, respectively.

Acknowledgement This research was supported by the Program for the Training of Graduate Students in Regional Strategic Industries and Regional Innovation Center (RIC) Program which was conducted by the Ministry of Commerce, Industry and Energy of the Korean Government.

References

1. J. Long, H. Chen, Z. Meng, Mater. Sci. Eng. **99**, 445 (2003) doi:10.1016/S0921-5107(02)00455-5
2. G.-M. Lee, *Agency for Technology and Standards, Industry and Energy of the Korean Government*, Seminar on EU product-related regulations, pp. 6. (2004)
3. H. Nagata, T. Takenaka, J. Eur. Ceram. Soc. **21**, 1299 (2001) doi:10.1016/S0955-2219(01)00005-X
4. G.A. Smolenskii, V.A. Isupov, A.I. Agranovskaya, N.N. Krainik, Sov. Phys.-Solid State (Engl. Trans.) **2**, 2651 (1961)
5. K. Sakata, Y. Masuda, Ferroelectrics **7**, 347 (1974) doi:10.1080/00150197408238042
6. T. Takenaka, K. Sakata, K. Toda, Ferroelectrics **106**, 375 (1990)
7. T. Takenaka, K. Maruyama, K. Sakata, Jpn. J. Appl. Phys. **30**, 2236 (1991) doi:10.1143/JJAP.30.2236
8. H. Nagata, T. Takenaka, Jpn. J. Appl. Phys. **36**(Part I), 6055 (1997) doi:10.1143/JJAP.36.6055
9. H. Nagata, T. Takenaka, Jpn. J. Appl. Phys. **37**, 5311 (1998) doi:10.1143/JJAP.37.5311
10. A. Sasaki, T. Chiba, Y. Mamiya, E. Otsuki, Jpn. J. Appl. Phys. **38**, 5564–5567 (1999) doi:10.1143/JJAP.38.5564
11. H. Nakata, N. Koizumi, T. Takenaka, Key Eng. Mater. **169–170**, 37–40 (1999)
12. T. Wada, K. Toyoike, Y. Imanaka, Y. Matsuo, Jpn. J. Appl. Phys. **40**, 5703 (2001) doi:10.1143/JJAP.40.5703
13. Y.M. Li, W. Chen, Q. Xu, J. Zhou, H.J. Sun, M.S. Liao, J. Electroceram. **14**, 53 (2005) doi:10.1007/s10832-005-6584-2
14. R. Zuo, C. Ye, X. Fang, J. Li, J. Eur. Ceram. Soc. **28**, 871 (2008) doi:10.1016/j.jeurceramsoc.2007.08.011
15. B.J. Chu, D.R. Chen, G.R. Li, Q.R. Yin, J. Eur. Ceram. Soc. **22**, 2115 (2002) doi:10.1016/S0955-2219(02)00027-4
16. Y.G. Wu, H.L. Zhang, Y. Zhang, J.Y. Ma, D.H. Xie, J. Mater. Sci. **38**, 987 (2003) doi:10.1023/A:1022333427521
17. H. Nagata, M. Yoshida, Y. Makiuchi, T. Takenana, Jpn. J. Appl. Phys. **42**, 7401 (2003) doi:10.1143/JJAP.42.7401
18. L. Wu, D.Q. Xiao, D.M. Lin, J.G. Zhu, P. Yu, Jpn. J. Appl. Phys. **44**, 8515 (2005) doi:10.1143/JJAP.44.8515
19. A. Herabut, A. Safari, J. Am. Ceram. Soc. **80**, 2954 (1997) doi:10.1111/j.1151-2916.1997.tb03219.x
20. H.D. Li, C. Feng, P.H. Xiang, Jpn. J. Appl. Phys. **42**, 7387 (2003) doi:10.1143/JJAP.42.7387
21. H.D. Li, C.D. Feng, W.L. Yao, Mater. Lett. **58**, 1194 (2004) doi:10.1016/j.matlet.2003.08.034
22. X. Zhou, H.S. Gu, Y. Wang, W.Y. Li, T.S. Zhou, Mater. Lett. **59**, 1649 (2005) doi:10.1016/j.matlet.2005.01.034
23. IRE Standards on Piezoelectric Crystals, *Measurements of Piezo. Ceram.*, proc. IRE **49**, 1161 (1961)
24. R.D. Shannon, Acta Crystallogr. **A32**, 751 (1976)
25. S.E. Park, S.J. Chung, J. Am. Ceram. Soc. **79**, 1290 (1996) doi:10.1111/j.1151-2916.1996.tb08586.x
26. B. Jaffe, *Piezoelectric ceramics* (Academic, New York, 1971), pp. 148–160
27. S. Säid, J.P. Mercurio, J. Eur. Ceram. Soc. **21**, 1333 (2001) doi:10.1016/S0955-2219(01)00012-7
28. J.R. Gomah-Pettry, S. Säid, P. Marchet, J.P. Mercurio, J. Eur. Ceram. Soc. **24**, 1165 (2004) doi:10.1016/S0955-2219(03)00473-4
29. M.S. Yoon, H.M. Jang, J. Appl. Phys. **77**(8), 3991 (1995) doi:10.1063/1.359510